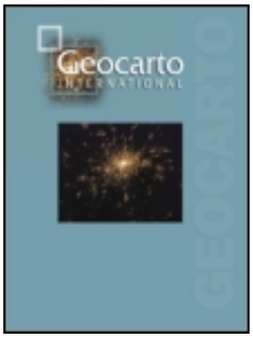

Geocarto International

ISSN: 1010-6049 (Print) 1752-0762 (Online) Journal homepage: https://www.tandfonline.com/loi/tgei20

Estuarine sediment deposition during wetland restoration: A GIS and remote sensing modeling approach

Michelle Elizabeth Newcomer, Amber Jean Michael Kuss, Tyler Ketron, Alex Remar, Vivek Choksi & J. W. Skiles

To cite this article: Michelle Elizabeth Newcomer, Amber Jean Michael Kuss, Tyler Ketron, Alex Remar, Vivek Choksi & J. W. Skiles (2014) Estuarine sediment deposition during wetland restoration: A GIS and remote sensing modeling approach, Geocarto International, 29:4, 451-467, DOI: 10.1080/10106049.2013.798356

To link to this article: https://doi.org/10.1080/10106049.2013.798356

© 2013 The Author(s). Published by Taylor & Francis

Published online: 14 Jun 2013.

Submit your article to this journal

Article views: 1879

View related articles

View Crossmark data

Citing articles: 5 View citing articles

Full Terms & Conditions of access and use can be found at
https://www.tandfonline.com/action/journalInformation?journalCode=tgei20

Geocarto International, 2014
Vol. 29, No. 4, 451–467, http://dx.doi.org/10.1080/10106049.2013.798356

Estuarine sediment deposition during wetland restoration: a GIS and remote sensing modelling approach

Michelle Elizabeth Newcomer[a]*, Amber Jean Michael Kuss[a], Tyler Ketron[b], Alex Remar[c], Vivek Choksi[d] and J. W. Skiles[e]

[a]*NASA DEVELOP National Program, NASA Ames Research Center, Moffett Field, USA* [b]*Earth Systems Program, Stanford University, Palo Alto, CA, USA;* [c]*Department of Geography, University of Delaware, Newark, NJ, USA;* [d]*Electrical Engineering, Stanford University, Palo Alto, CA, USA;* [e]*Biospheric Science Branch, NASA Ames Research Center, Moffett Field, USA*

(*Received 22 August 2012; final version received 18 April 2013*)

Restoration is currently underway in the industrial salt flats of San Francisco Bay, California. Remote sensing of suspended sediment concentration and other geographical information system predictor variables were used to model sediment deposition within recently restored ponds. Suspended sediment concentrations were calibrated to reflectance values from Landsat TM 5 and ASTER satellite image data using three statistical techniques – linear regression, multivariate regression and artificial neural network (ANN) regression. Multivariate and ANN regressions using ASTER proved to be the most accurate methods, yielding r^2 values of 0.88 and 0.87, respectively. Predictor variables such as sediment grain size and tidal frequency were used in the marsh sedimentation (MARSED) model for predicting deposition rates. MARSED results show a root-mean-square deviation of 66.8 mm ($<1\sigma$) between modelled and field observations. This model was applied to a pond breached in November 2010 and indicated that the pond will reach sediment equilibrium levels after 60 months of tidal inundation.

Keywords: suspended sediment concentration; remote sensing; MARSED; wetlands; GIS

Introduction

The San Francisco Bay Estuary, with a total area of approximately 4143.9 km^2, is the largest estuary in the USA. Development of the San Francisco Bay Estuary during the last 200 years has transformed nearly 90% of historical wetland habitats into agricultural fields and industrial salt production ponds (Philip Williams & Associates Ltd. & Faber 2004). The South Bay Salt Pond Restoration Project (SBSPRP), the largest and most complex wetland restoration effort on the West Coast of the USA, will convert approximately 6070 hectares of salt production ponds to restored wetland habitats (Takekawa et al. 2005). Understanding long-term sediment dynamics within the South Bay is critical for proper accumulation estimates and subsequent restoration management strategies in newly breached salt ponds (Foxgrover et al. 2007; Trulio et al. 2007). Sediment accumulation rates of breached salt ponds are directly influenced by

*Corresponding author. Email: michelle.e.newcomer@nasa.gov

© 2013 The Author(s). Published by Taylor & Francis.
This is an Open Access article. Non-commercial re-use, distribution, and reproduction in any medium, provided the original work is properly attributed, cited, and is not altered, transformed, or built upon in any way, is permitted. The moral rights of the named author(s) have been asserted.

suspended sediment concentrations (SSCs), water flow paths, and tidally-driven sediment re-suspension (Philip Williams & Associates Ltd. & Faber 2004). Marshland rise within the breached salt ponds allows plant colonization and establishment of a healthy wetland ecosystem (Philip Williams & Associates Ltd. 2005). Currently, the SBSPRP requires continued monitoring of newly breached salt ponds for three main reasons: to understand sediment dynamics, to estimate the time required for establishment of vegetation in newly-breach ponds, and to identify potential changes in adaptive management strategies for restoration.

Satellite image processing has previously been used to calibrate image-based reflectance values to *in situ* measurements of SSCs in the visible and near-infrared spectral range (Munday & Alföldi 1979; Chen et al. 1992; Baban 1995; Miller & McKee 2004; Chen et al. 2006; Brodie et al. 2010; Xuejie & Damen 2010). Previous studies report strong correlations between reflectance values and *in situ* turbidity (another measure of suspended sediment) using a linear analysis in the 600–700 nm range ($r^2 = 0.72$) (Miller & McKee 2004; Chen et al. 2006), while other studies report strong correlations in the 600–900 nm range ($r^2 = 0.79$) using a linear and multivariate analysis (Pavelsky & Smith 2009).

Once SSCs are accurately mapped for the study area, deposition rates and cumulative totals can be calculated. Sediment deposition is a function of the SSC, settling velocity, bulk density, and water velocity (Temmerman et al. 2004). Temmerman et al. (2003) modified an algorithm developed by Krone (1987) to predict sediment deposition using these known variables and was able to predict sediment deposition in growing marsh ecosystems at point locations of known SSC. This current study used point locations of SSC to calibrate satellite imagery, providing a spatially comprehensive distribution of SSCs within Ponds A21–A6. Accurately mapping SSCs from remotely sensed images provided a method for determining sediment concentrations without disturbing ecologically sensitive areas.

Field methods are also necessary for accurate calibration of satellite imagery. Various studies have developed methods for monitoring *in situ* sediment accumulation rates, with a wide-range of techniques and accuracy. Installed monitoring devices, such as sediment traps (Gardner et al. 1980; Bale 1998), graduated pins (Reed 1989; Cahoon & Lynch 1997; Callaway et al. 2009), anchored tiles (Reed 1989; Pasternack & Brush 1998) and sediment erosion tables (Boumans & Day 1993; Childers et al. 1993; Cahoon et al. 2002), are inexpensive and effective methods for estimating accumulation rates, but provide limited sampling points. SSC estimates are often used to indirectly measure sediment accumulation rates, and they can be obtained through *in situ* measurements and remote sensing techniques (Stumpf & Pennock 1989; Froidefond et al. 1993; Ruhl et al. 2001; Li et al. 2003; Miller & McKee 2004).

Modelling techniques can be used to calculate future and current sediment accumulation rates, and some models account for factors including wetland age, surface elevation, and sea level fluctuations (Allen 1990; French & Spencer 1993; French et al. 1995; Allen 1997; Temmerman et al. 2003; Temmerman et al. 2004). A zero-dimensional time-stepping marsh sediment deposition model (MARSED) has been used to predict wetland development based on particle settling velocity, time dependent SSCs, and sediment bulk density (Krone 1987; Temmerman et al. 2003; Temmerman et al. 2004).

In this study, combined *in situ* and remote sensing applications were used to monitor sediment accumulation in newly breached salt production ponds in the South San Francisco Bay. Remote sensing methods used optical imagery from the Landsat-5 Thematic Mapper (TM) satellite and the Advanced Spaceborne Thermal Emission and

Reflection Radiometer (ASTER) satellite to monitor SSCs within this region. Additionally, *in situ* SSC samples were collected during satellite overpasses to generate an applied relation between spectral observations and ground-truth data. This study represents the first attempt to use these methods within the adaptive management strategy of restoration for the SBSPRP. Continued monitoring of estuarine sediment accumulation will provide temporal and spatial development predictions for each phase of the restoration process.

Materials and methods

Study site

Tidal marshes are among the most highly productive ecosystems on the planet (Kelly & Tuxen 2009). The South Bay salt ponds, located at the southern end of San Francisco Bay (Figure 1), lie on the Pacific flyway, providing roosting and over-wintering sites for migratory bird species, and habitat for waterfowl, shorebirds, and mammals (Siegel & Bachand 2002). This highly productive area is created through the conveyance of the Sacramento and San Joaquin rivers into the Pacific Ocean (Looker 2011). Flows in this area are highly seasonal, with runoff mostly occurring in the rainy winter season (Looker 2011). Groundwater is also an important component of the hydrological system in this region, and provides a source of freshwater replenishment; however, urbanization of the area has led to degradation of water quality in this region. In the South Bay, freshwater enters through the Coyote Creek Tributary and delivers sediment to the Alviso Ponds. Additionally, the San Francisco Bay is located in a region with a Mediterranean climate, with warm summers and mild winters. Approximately 85% of the annual precipitation occurs from November to April (Looker 2011). In March of 2006, the US Fish and Wildlife Service Don Edwards National Wildlife Refuge and the Santa Clara Valley Water District initiated tidal pond inundation in Pond A21 (Callaway et al. 2009). The levees of the Pond A21 (Figure 1) were breached, allowing daily tidal flow for the first time in over 100 years with the goal of providing natural sedimentation processes to restore the tidal marsh habitat for successful vegetation reestablishment (Callaway et al. 2009).

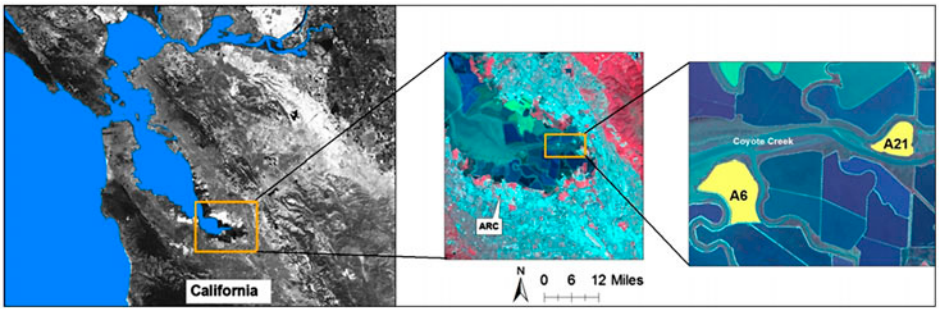

Figure 1. Study location in the Alviso Complex in the San Francisco Bay, California. Ponds A21 and A6 are shown in yellow. Note also the location of Coyote Creek and NASA Ames Research Center.

Experimental design

Sediment deposition was modelled for Pond A21 for the three years after the levees were breached in March, 2006 (Figure 1) (Newcomer et al. 2011). The model was further applied to Pond A6 (discussed below) following the methods outlined by Newcomer et al. (2011). Pond A6 was breached in November 2010 and a high tide satellite image was obtained on 5 January 2011 from the Landsat TM 5 satellite. Landsat TM 5 has a pixel size of approximately 30 m × 30 m and acquires data over the same location approximately every two weeks at approximately 10 am (WIST 2010). Additional image acquisition dates and bands used are discussed below.

Satellite remote sensing

Landsat TM 5 and ASTER were used in this study specifically to map suspended sediment in the South San Francisco Bay (USGS 2010a; WIST 2010). Both ASTER and Landsat TM 5 were chosen for this study because of the availability of cloud-free images, the breadth of bands available and the range of resolution provided by the two. All satellite images were radiometrically corrected to reflectance and re-projected to the UTM WGS 84 North projection to ensure tonal and spatial comparability between each scene. To create SSC maps, Landsat TM 5 and ASTER images were first imported into a geographical information system (GIS) environment (ArcGIS). Reflectance values from Band 1, 2 and 3 of ASTER (520–600, 603–690 and 780–860 nm, respectively) were calibrated with SSC values using two scenes (Table 1). Reflectance values from Band 1, 2, 3, and 4 of Landsat TM 5 (450–520, 520–600, 630–690 and 760–900 nm respectively) were calibrated with SSC values using two scenes, and the other three scenes were used for prediction (Table 1).

To calibrate the remotely sensed images to SSC values, three statistical techniques were used. Linear, multivariate, and artificial neural network (ANN) regressions were compiled for both sensors to determine the best statistical technique for correlation with SSCs and to allow a robust analysis of the thresholds of SSC for maximum and minimum sediment deposition prediction. Landsat TM 5 and ASTER images were calibrated using data from the historical USGS Water Quality of San Francisco Bay monitoring program (USGS 2007, 2010b) and from field samples. The scenes selected in Table 1 were based on the availability of an overpass that corresponded with a cloud-free day and correlated with the day of the historical USGS samples and the field samples. Values were determined at both the original resolution and at an averaged resolution (a 3 × 3 grid) to reduce signal noise. Additional inputs of seasonal variations in SSCs, distance from the levee breach, bulk density, settling velocity, initial marsh height, time of inundation, tidal frequency, and a high-volume array of SSC data points (obtained from the satellite-produced images) were used in the MARSED model.

Table 1. Satellite sensors used to detect SSCs and corresponding dates.

Sensor	Bands used	Wavelengths (nm)	Resolution (m)	Dates used	Image source
ASTER on Terra	1,2,3	520–860	15	10/8/04, 10/29/09	Glovis (USGS 2010a)
Landsat 5 TM	1,2,3,4	405–900	30	8/18/94, 8/22/07, 8/27/09, 7/5/10, 1/5/11	Glovis

After calibrating the satellite imagery using the regression equations, the SSC maps were input into the MARSED model to predict deposition in Pond A21 for three years post-breach. Modelled marsh accumulation values were then compared to previously documented point measurements of sediment accumulation heights in the breached Pond A21 (Callaway et al. 2009) to assess model accuracy. Pond A21 was used in the model due to the previously acquired point measurements provided in Callaway et al. (2009), which provided a baseline for comparison with the modelled estimates. Once the modelled values for Pond A21 were within reasonable tolerance (± 10%) to previously documented point measurements, the model was used to predict deposition for Pond A6, which was breached in November 2010.

Field methods

Surface water samples for suspended sediment analysis were collected at 24 random locations in the South Bay over the course of two field days that corresponded with Landsat TM 5 and ASTER overpasses. Since the sampling locations required boat access, they were chosen in locations of the deep water channel where the boat would not affect SSC values. SSC samples were obtained by placing a 1L closed container into the water and opening the container at arm's length to fill with water just below the surface. Samples were processed at the USGS Western Coastal and Marine Geology Laboratory (WCMGL) to determine SSC values. In addition, sediment samples were collected from Pond A21 to characterize the physical properties (density, type, and size) of sediment in the South Bay. These samples were taken at five representative locations along the perimeter and seven locations on the interior of the pond. Samples were obtained on the marsh surface by using an extendable instrument (extended 15 feet) with a scoop to allow for a sediment grab sample in areas that we could not reach by foot. Each sample was processed at the WCMGL for grain size distribution, settling velocity, and organic content (Table 2). A value for bulk density was generated from a reference density data-set of clay and mud densities (SI Metric 2010). These characteristics, along with SSCs, are inputs to the MARSED model (Temmerman et al. 2003; Temmerman et al. 2004).

Table 2. Variables used in the MARSED model, the field collection method for each variable and the corresponding laboratory processing techniques.

Variable	Field collection method	Laboratory processing technique
Suspended sediment concentration (mg/L)	Water samples from South Bay	Filtration
Grain size distribution	Sediment samples from Pond A21	Coulter LS100Q using laser diffraction
Settling velocity (cm/s)	Sediment samples from Pond A21	Modified Gibbs equation (Gibbs et al. 1971)
Organic carbon content (% organic carbon)	Sediment samples from Pond A21	CO_2 coulometer and combustion chamber

USGS continuous monitoring stations and monthly cruises

In addition to the field collected SSC samples, historical SSC data-sets were obtained from the USGS's Water Quality and Continuous Monitoring Stations of San Francisco Bay database for sampling stations 30–36, south of the San Mateo Bridge (USGS 2007, 2010b). These additional data-sets provided us with a more comprehensive set of SSC values with which to correlate with the satellite images from 1994, 2007 and 2009. Outliers due to sensor interference from biological fouling, especially during summer months, were excluded (Buchanan & Lionberger 2007). Additionally, these data-sets were used to calculate seasonal trends of sediment influx to the South Bay. Seasonal mean averages were computed and compared to the 10-year average of 35.20 mg/L. The ratio between seasonal average SSCs and the 10-year average was calculated to be 1.08 for winter, 1.16 for spring, 0.95 for summer and 0.81 for fall. Most of the seasonal variation in SSCs can be explained by high rainfall in the winter and spring (NCDC 2010). Resuspension of sediments can also contribute to higher concentrations in the spring and summer months, due to stronger winds in the South Bay (Buchanan & Lionberger 2007). These coefficients were applied to seasonally adjust predicted SSCs in the MARSED model.

Marsh sediment deposition model (MARSED)

One goal of this study was to model sediment deposition in Pond A21 (Figure 1) and compare modelled results with the field data-set for sediment deposition collected by Callaway et al. (2009). To effectively model sediment accumulation over several tidal cycles and years, the MARSED model developed by Krone (1987) and modified by Temmerman et al. (2004) was implemented using ArcGIS to predict sediment accumulation for Pond A21, and then an accuracy assessment was run to verify simulated results from Equation (1).

$$\frac{dE}{dt} = \frac{dS(grain)}{dt} + \frac{dS(organic)}{dt} - \frac{dP}{dt} \tag{1}$$

where

dE/dt = rate of marsh height rise (m/year).
$dS(grain)/dt$ = rate of mineral sediment deposition (m/year).
$dS(organic)/dt$ = rate of organic content deposition (m/year).
dP/dt = resuspension/compaction (m/year).

Equation (1) was solved for dE/dt by summing the rates of deposition for mineral sediment and organic content and subtracting resuspension and compaction. Organic content was obtained from laboratory analysis and solving for the addition of sediment grains, $dS(grain)/dt$, required further calculation in Equation (2). Equation (2) provides the total grain deposition by calculating deposition for each tidal cycle and subsequently for each years. Equation (2) produced a final estimate of marsh evolution during the three years post-breach as a function of sediment concentration, settling velocity, and bulk density of the sediment grains (Krone 1987).

$$\frac{dS(grain)}{dt} = \int_{Year} \int_{Tide} \frac{w_s \times C(t) \times dt}{\rho} \tag{2}$$

where

$dS(grain)/dt$ = rate of mineral sediment deposition (m/year).

w_s = particle settling velocity (m/s).

$C(t)$ = time dependent sediment concentration from Equation (3) (kg/m^3), obtained using remote sensing.

ρ = dry bulk density of deposited sediment (kg/m^3).

To obtain the $C(t)$ term in Equation (2), the initial concentration value $C(0)$ was taken from the remotely sensed image, and then Equation (3) was solved for dC/dt with initial condition $t = 0$. Euler's method was used to compute $C(t)$ iteratively until it reached its final steady-state value. To initially model the changing sediment concentration with the incoming tide, Equation (3) was solved at time steps of $t = 0.001$s in Matlab (Krone 1987; Temmerman et al. 2003).

$$[h(t) - E]\frac{dC}{dt} = -w_s C(t) + [C(0) - C(t)]\frac{dh}{dt} \tag{3}$$

where

$h(t)$ = time dependent water surface elevation (m).

E = elevation of the marsh surface (m).

dC/dt = rate of sediment concentration change (kg/s).

w_s = particle settling velocity (m/s).

$C(t)$ = time dependant sediment concentration (kg/m^3).

$C(0)$ = initial sediment concentration (kg/m^3).

dh/dt = velocity of incoming flood tide (m/s).

For the purposes of this study, the Euler's method yielded a sufficient approximation to the final SSC value. The numerical approximation for solving Equation (3) at time steps of $t = 0.001$ s and 60,000 + iterations ensured a steady-state solution was reached. Euler's method was appropriate for solving Equation (3) because the Euler global error is proportional to the precision of the time step – approximately ±0.001 mg/L in this case (Zill & Cullen 2009). This error is insignificant to the overall SSC values because the accuracy of the laboratory-derived SSC is ±0.01 mg/L.

Marsh sedimentation is influenced by many variables including the time the pond is inundated, organic matter content, seasonal influences of sediment concentration, tidal velocity, water depth, sediment grain size and density, existing height of marshes, particle settling velocity, and distance from the levee breech. SSC was the most influential variable in this study and was calculated using an algorithm applied to the remote sensing images. For each pixel, a correlating SSC value was used as the initial condition ($C(0)$) and applied to Equation (3) to determine the final rate of concentration change (dC/dt). Once the rate of concentration change was obtained, the concentration at any specific time thereafter could be solved. The MARSED model was applied to Pond A6 in the Alviso complex, which was breached in November of 2010 (Figure 1). A 5 January 2011 Landsat TM 5 image was used to map SSCs because of an overpass on a day of high tide.

Statistical analysis

Three different statistical techniques were used to establish correlations between a range of SSC values (0–100 mg/L) and satellite reflectance values (Teodoro et al. 2008) – linear regression, multivariate regression and ANN regression. For linear regressions, the band

that produced the best statistical correlation for each sensor was determined and then used in subsequent calculations. For multivariate regressions and ANNs, all available visible and near-infrared bands were used. The ANN was implemented using an adaptive linear combiner (Wilde 2009). The ANN estimates the SSC by multiplying each band by a weight. After each iteration, the residual is calculated and the weights are adjusted until the error is minimized. Essentially, the ANN takes the data and learns from it until it produces the lowest possible error. Field SSC measurements as well as data from the USGS's Water Quality of the San Francisco Bay Project were correlated with reflectance values from multiple satellite images using all of these statistical techniques (USGS 2010b). The final values contained in the SSC maps were then used in the MARSED model to predict sediment deposition.

Sensitivity analysis

A sensitivity analysis of the MARSED model to different input variables was run to assess how some of the most important predictor variables change the trajectory of marsh equilibrium accumulation. The variables of tidal velocity, length of each time step and the time-length of slack during one tidal cycle were considered. These three variables influence the total amount of accumulation for each tidal cycle. The modelled data-set was compared to the field data-set and the sensitivity of the model to these three different variables was examined.

The velocity of the incoming tide is important to the model because of drag induced erosion. The grain size analysis indicated a large proportion of clay particles in the sediment which are susceptible to scour at low velocities; thus, three different model runs using different tidal velocities were considered to better understand outcomes on this variable. Additionally, tidal velocities change on a daily basis depending on the season and current meteorological conditions. Because we do not have access to velocity data on a daily time schedule, we used an average value for the time period of the study.

The length of each time step in the model can also change the SSC prediction value used to calculate deposition. To test the SSC sensitivity to the time step, and thus the final model convergence, Equation (3) was solved for each time step to retrieve the change in the SSC with time. Time steps of 0.01, 1, 2.5, and 5 s were chosen to test model sensitivity. Lastly, the time-length of slack during one tidal cycle was considered.

The period of slack is very important to marsh accumulation: without a significant amount of time for sediment to deposit, acceptable rates of marsh accumulation will not occur. Three different slack times – 0.5, 1, and 1.5 h – were chosen to test the model sensitivity and the calculation of deposition rates.

Results

Field and laboratory results

Average values from the field samples that were used in the MARSED model are shown in Table 3. These field values were obtained in an initial reconnaissance study by Newcomer et al. 2011. Average surface SSCs for Pond A21 were 46.16 mg/L. This is consistent with the values provided by the multivariate regression for Pond A21 using the satellite images. The sediment is dominated by clay sized particles – 92% of particle diameters fall below 16 μm (Krumbein & Sloss 1963). Organic content is also quite low in this field environment.

Table 3. Average values of the field data collected in Pond A21. All data were analysed in the USGS Western Coastal Marine Geology Laboratory.

Variable	Average value
Surface suspended sediment concentration (mg/L)	46.16
Grain size (μm)	4.72
Settling velocity (m/s)	5.06×10^{-3}
Organic carbon content (% organic carbon)	2.08
Bulk density (kg/m^3)	1600

Suspended sediment prediction results

The accuracy of detecting SSCs through the use of remote sensing is dependent on many factors including the resolution of the satellite image, the ability to acquire and process the image with corresponding *in situ* SSC values and hydrodynamic influences. The two remote sensing instruments used in this study (ASTER and Landsat TM 5) show varying accuracies in correlating reflectance values with SSCs (Table 4). Reflectance values in clear water are generally zero, and predictably increase with increasing SSCs (mg/L) (Figure 2). Similar results are also shown by Li et al. (2003). Regressions effectively correlated pixel values with SSCs in each of the sensors, and were subsequently applied to each satellite image in ArcGIS to create temporal maps of SSC data, effectively gaining the variable $C(0)$ for use in Equation (3), then converted to a deposition rate in mm/year using Equation (2). The most effective linear regression for SSC correlations from ASTER and Landsat TM 5 used band 3, which is consistent with previous studies using visible spectrum imagery (630–690 nm) (Table 3). Multivariate and ANN regressions using ASTER imagery proved to be the most accurate correlation methods, yielding r^2 values of 0.88 and 0.87, respectively (Table 3). ASTER produced the most accurate results in correlating SSCs, which was expected due to its high (15 m) resolution.

MARSED GIS model results

Root-mean-square deviation (RMSD) was used to measure the difference between marsh accumulation values computed by the model and field values collected by Callaway et al. (2009) (Table 4). Linear regression with band 3 of ASTER provided the most accurate results, yielding a RMSD of 66.84 mm (Table 4). This is less than 3 inches of deviation, providing reasonable error and accuracy for predicting marsh sedimentation at local ponds in the South Bay.

Table 4. Regressions are shown from the linear, multivariate and ANN statistical techniques for predicting SSCs. RMSD (mm) calculated between modelled and field results is also shown from comparisons with the field results. Note that the most accurate predicted data-set was derived from ASTER linear regression with an RMSD of 66.84 mm.

Sensor	Linear	Multivariate	ANN
Regressions			
Landsat 5 TM	0.83 (Band 3)	0.84	0.69
ASTER	0.65 (Band 3)	0.88	0.87
RMSD (mm)			
Landsat 5 TM	120.41	186.84	131.83
ASTER	66.84	97.94	82.32

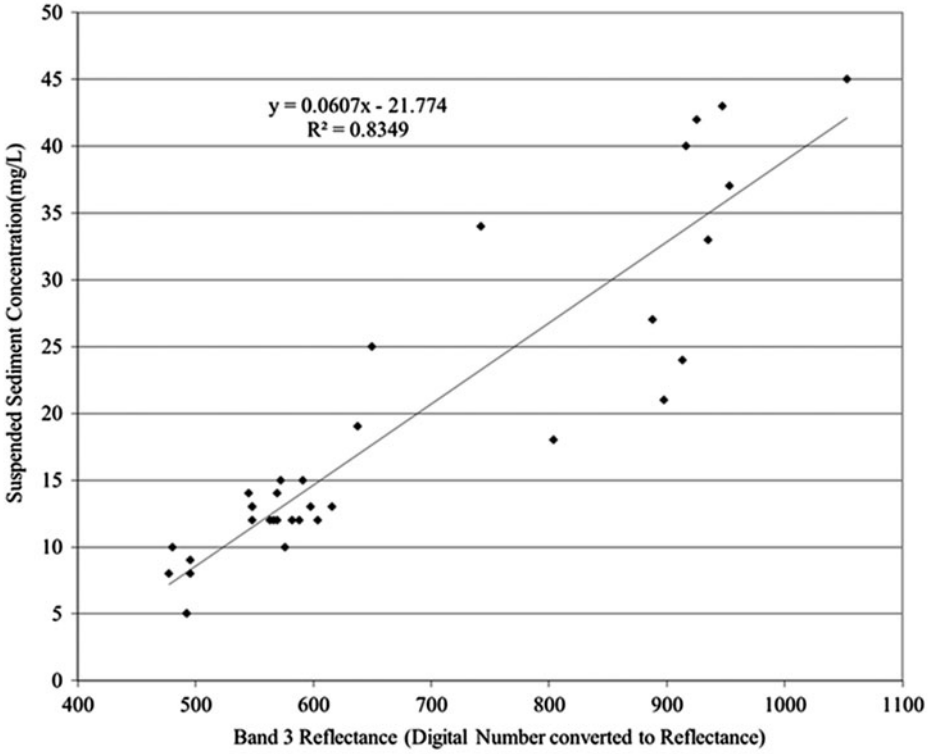

Figure 2. Linear regression between SSCs (from USGS and field samples) and reflectance values from Landsat TM. Landsat band 3 (630–690 nm) reflection correlated strongly with suspended sediment concentration.

Predicting deposition in Pond A6

Sediment deposition was predicted for Pond A6 in the Alviso complex using the MARSED model, and cumulative deposition is shown in Figure 3. An initial run of the model with the same rates of deposition and initial conditions as for Pond A21 did not yield marsh equilibrium levels to provide a stable habitat for vegetation colonization within a 36-month time frame. The model was then run for a longer time frame, yielding equilibrium levels after 60 months.

Model sensitivity

When considering the model sensitivity to tidal velocity (Figure 4), the time until marsh equilibrium can vary significantly. The field data line shows the true values for marsh accumulation over time measured by field parameters (Callaway et al. 2009). The high, medium, and low tidal velocity curves correspond to different marsh accumulation rates for each run. The incoming tidal velocity was estimated to be 7, 10, and 12 mm/s for the lowest, medium, and highest tidal velocities, respectively. For the final model run, the lowest tidal velocity of 7 mm/s was used.

Model sensitivity results to the time step are shown in Figure 5. A time-step of 5 s produces larger errors initially, but eventually results in the same concentration value as

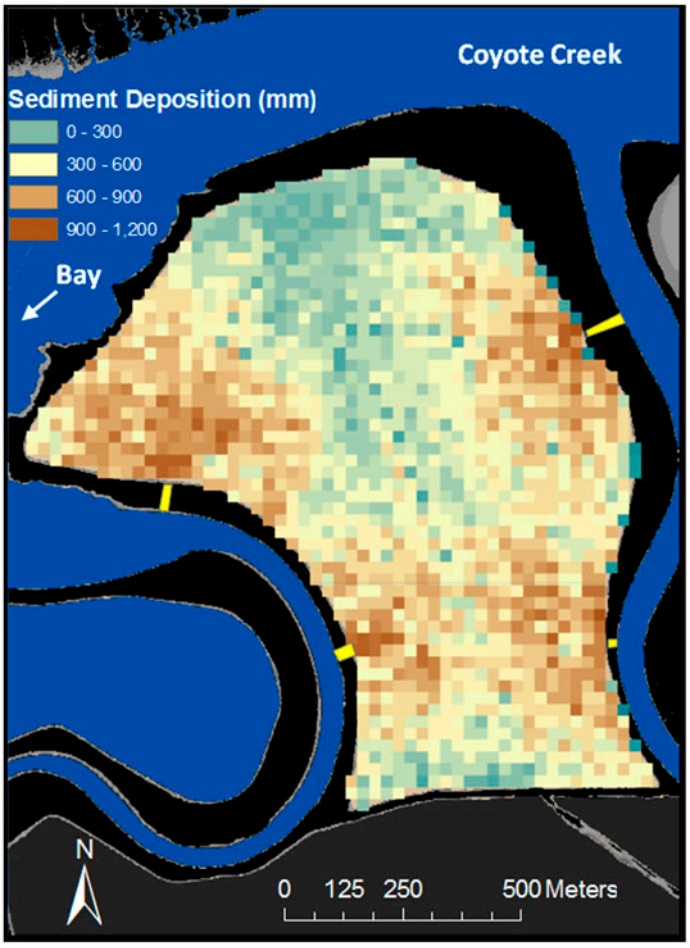

Figure 3. Pond A6 showing sediment deposition in mm. The locations of the levee breaches (yellow) are indicated. Also, the South Bay flows into Coyote Creek near Pond A6.

the other time steps. For this analysis, a time-step of 0.001 s was used. Because accumulation of a marshland occurs at timescales much larger than those producing errors here, a time step on or under the order of hours could have been used.

Model deposition sensitivity to changes in the period of slack is shown in Figure 6. A slack time of 0.5 h produces less than half of the amount of deposition compared to a 1.5 h slack time. The total time of slack was chosen to be 1.5 h due to the average slack time observed in the study area (NOAA 2011).

Discussion

Field results of SSC values compared well with the satellite image calibration of SSC values. The field validation using multivariate correlation provides the best possible SSC map for input into the MARSED model. Field values of SSC content were necessary for a consistent and accurate calibration of the satellite imagery for input to the MARSED model. The low organic content of sediment in our samples can be attributed

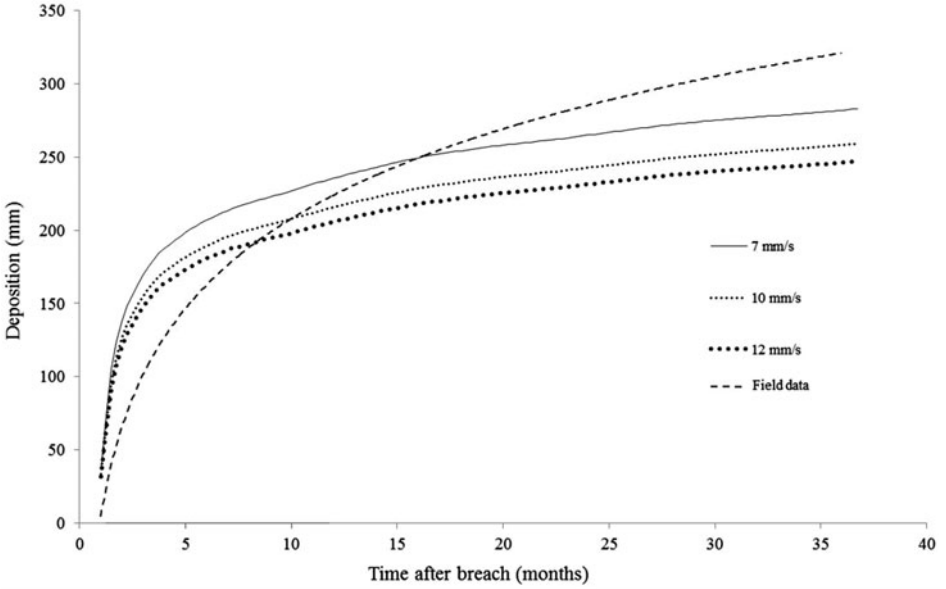

Figure 4. MARSED model sensitivity to the input tidal velocity. Deposition is cumulative over the three years post-breach.

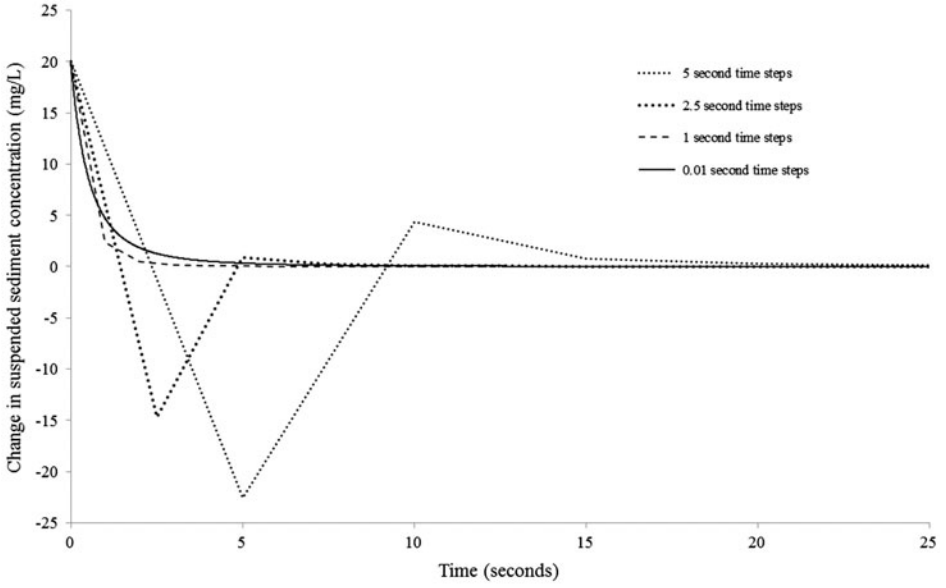

Figure 5. Sensitivity of the MARSED model to the length of the time steps. Time steps of 0.01 s produces a relatively more stable curve than the other, and for accuracy purposes, a time step of 0.001 s was used in this study.

to the fact that Pond A21 is a continuously developing marsh with little biological activity. Thus, this variable did not contribute significantly to overall deposition totals.

When comparing the three regression techniques for calculating SSC values, it was found that band 3 was the most accurate using the linear regression method with Landsat TM 5 imagery. Multivariate and ANN regressions using ASTER imagery, however,

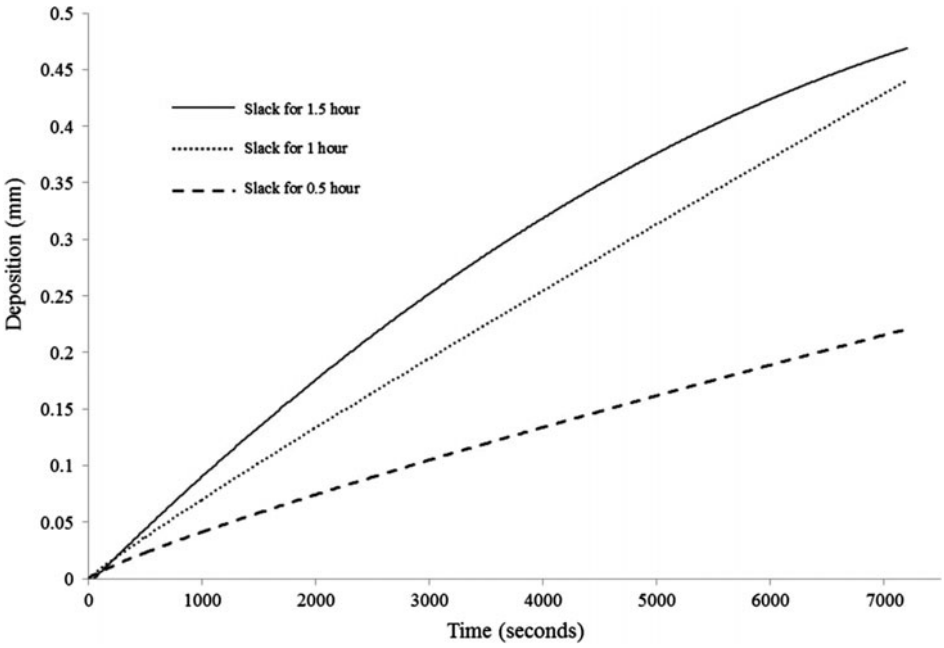

Figure 6. Sensitivity of the MARSED model to the time of the slack period. Because tides vary each day, and because the ponds are shielded from large variations in tides, a slack period of 1.5 h was chosen.

proved to be the most accurate correlation method overall, and this is attributed to the more detailed resolution (smaller pixel size) of ASTER compared with Landsat TM 5 as well as the higher number of bands across which the field data can be compared. However, the linear regression method using ASTER produced the lowest regression value, and this can be attributed to the lack of field data for the overpass of the ASTER sensor as well as the fact that only one band could be used for each regression. While many previous studies have demonstrated the value of using the visible spectrum for SSC analysis, our study considered spectra outside of the visible region and used a multivariate statistical technique with multiple bands. A multivariate technique allows for a broader use of the available data and considers a wavelength spectrum that is not widely used in this field.

The MARSED model can accurately predict marsh sedimentation in the newly breached salt ponds in the South San Francisco Bay. The accuracy of the MARSED model is dependent on field data and GIS inputs. In the case of prediction using ASTER, the linear technique produced the lowest RMSD for the model, whereas multivariate regression produced the best correlation between SSC and reflectance (Table 4). This was surprising – linear regression, being the simplest statistical method used, was not expected to produce the most accurate marsh accumulation estimates. This discrepancy could have resulted from bias in the model, which systematically overestimated marsh accumulation. This overestimation most likely arose because the model does not account for compaction or resuspension of settled sediment processes, which inhibit marsh elevation rise. Resuspension may be wind generated (driven by shear velocity and water depth) or tidally generated (when ebb tide moves water and sediment out of the ponds).

The inherent error of the model can also be attributed to the deviation of the reflectance values from the true SSC values. Reflectance values are measured to the fifth decimal place, whereas SSCs are reported to the second decimal place. This discrepancy could result in multiple reflectance values for the same SSC value, thus increasing error in the analysis. The cumulative marsh sedimentation curve is shown in Figure 4. The marsh initially rises rapidly, but sedimentation rates slow as the marsh sediment nears a stable height relative to sea-level that allows for vegetation colonization. The height of marsh growth will vary with the initial elevation of the pond; however, once equilibrium with sea-level is reached, the marsh will no longer accumulate sediment.

The MARSED model predicted that Pond A6 would reach equilibrium in approximately 60 months. One interpretation for the longer time frame compared with other ponds is that a longer time frame was necessary because SSCs are consistently lower (by about half) around A6 than around A21, leaving less sediment for deposition and resulting in lower marsh accumulation rates in A6. The location of the levee breaches also factored into the longer time frame for marsh establishment in A6 (Figure 3). Pond A6 has two breaches along a slough divergent from the relatively calm Coyote Creek, as well as two breaches connecting the Pond to the relatively strong tidal currents of the South Bay. The tidal influences from the breach on the west side of Pond A6 may increase the potential for erosion and further inhibit marsh accumulation from the rates observed in Pond A21. The initial height of Pond A6 also factors into the time frame required for the marsh to reach equilibrium. Pond A6 has experienced much more subsidence and compaction than other ponds and initially had lower elevations. Because of its low initial elevation, Pond A6 requires more sediment deposition to reach equilibrium.

Sensitivity analysis results show that the time of slack and the settling velocity are variables that cause model sensitivity. We assumed the lowest tidal velocity in our model because of the geometry of the study area. The tidal velocities we chose for the analysis are slow relative to typical velocities of tides and to velocities outside of the pond breaches. Since the ponds fill up from multiple input points, we assumed that flow in through these points would sufficiently suppress the tidal velocity, allowing for sediment accumulation. Small changes in the assumed tidal velocity produced significant changes in the accumulation. For example, the lowest tidal velocity produced the highest amount of marsh accumulation because sediments can only settle when conditions are at or near slack.

Although the model produced results that are applicable to other wetland restoration efforts, outliers in the error of the MARSED model's predictions indicate a need for further assessment of environmental variables. Four outliers greatly underestimated sediment accumulation in the model, and were not included in the RMSD calculations. These outliers corresponded with locations along the south-eastern perimeter of Pond A21, where unaccounted influences from the tidal channel and from pond geometry may have significantly heightened true marsh accumulation. When outliers were excluded, the model's RMSD of 66.84 mm fell within one standard deviation of actual accumulation values. Due to highly accurate depositional estimates, the model is a useful tool for studying future wetland restoration efforts; however, the sensitivity of the model should be considered for future use in other wetland ecosystems.

Conclusions

In this study, SSCs were successfully calibrated to remote sensing reflectance values using three statistical techniques: linear regression, multivariate regression and ANN

regression. Multivariate correlations with ASTER provided the best r^2 value (0.88). The output suspended sediment maps were then used in the MARSED model to predict sediment deposition for Pond A21. Model results show excellent correlation with observed sedimentation rates from Pond A21 with a RMSD of 66.8 mm (approximately 2.6 inches). Overall, the model is an accurate predictor of sedimentation for the South San Francisco Bay salt ponds and can be a useful and successful tool for future management decisions. The model can aid restoration managers not only in deciding the ideal location for a breach, but also in providing time estimates for a newly breached pond to reach equilibrium levels.

Acknowledgements

This research was funded by the NASA DEVELOP National Program. We thank Dr Randy Berthold, John Preston and Matt Linton for making the NASA DART boats available for our sampling campaign. We also thank Dr Mike Torresan and Angela Lam for providing the USGS facilities for our sediment analysis. We also thank Dr Karen Grove, Erin Justice, Dr Charles Williams, Brad Lobitz and Dr David Freyberg for their help and support with this project. The team also acknowledges the ASTER science team and the Landsat TM 5 science team for providing the data and support. The team acknowledges the helpful review provided by Cindy Schmidt and Christine Scofield and the comments provided by anonymous reviewers.

References

Allen J. 1990. Salt-marsh growth and stratification: a numerical model with special reference to the Severn Estuary, southwest Britain. Mar Geol. 95:77–96.

Allen J. 1997. Simulation models of salt-marsh morphodynamics: some implications for high-intertidal sediment couplets related to sea-level change. Sed Geol. 113:211–223.

Baban SMJ. 1995. The use of Landsat imagery to map fluvial sediment discharge into coastal waters. Mar Geol. 123:263–270.

Bale A. 1998. Sediment trap performance in tidal waters: comparison of cylindrical and conical collectors. Cont Shelf Res. 18:1401–1418.

Boumans R, Day J. 1993. High precision measurements of sediment elevation in shallow coastal areas using a sedimentation–erosion table. Estuaries Coasts. 16:375–380.

Brodie J, Schroeder T, Rohde K, Faithful J, Masters B, Dekker A, Brando V, Maughan M. 2010. Dispersal of suspended sediments and nutrients in the Great Barrier Reef lagoon during river-discharge events: conclusions from satellite remote sensing and concurrent flood-plume sampling. Mar Freshw Res. 61:651–664.

Buchanan P, Lionberger MA. 2007. Summary of suspended-sediment concentration data, San Francisco Bay, California, water year 2005. Reston (VA): US Geological Survey Data Series 282; p. 49.

Cahoon DR, Lynch JC. 1997. Vertical accretion and shallow subsidence in a mangrove forest of southwestern Florida, USA. Mangroves Salt Marshes. 1:173–186.

Cahoon D, Lynch J, Hensel P, Boumans R, Perez B, Segura B, Day J, Jr. 2002. High-precision measurements of wetland sediment elevation: I recent improvements to the sedimentation–erosion table. J Sediment Res. 72:730–733.

Callaway JC, Parker VT, Schile LM, Herbert ER, Borgnis EL. 2009. Dynamics of sediment accumulation in Pond A21 at the Island Ponds. Oakland (CA): California State Coastal Conservancy; p. 66.

Chen Z, Curran PJ, Hansom JD. 1992. Derivative reflectance spectroscopy to estimate suspended sediment concentration. Remote Sens Environ. 40:67–77.

Chen Z, Hu C, Muller-Karger F. 2006. Monitoring turbidity in Tampa Bay using MODIS/Aqua 250-m imagery. Remote Sens Environ. 109:207–220.

Childers D, Sklar F, Drake B, Jordan T. 1993. Seasonal measurements of sediment elevation in three mid-Atlantic estuaries. J Coastal Res. 9:986–1003.

Foxgrover A, Jaffe B, Hovis G, Martin C, Hubbard J, Samant M, Sullivan S. 2007. 2005 Hydrographic survey of South San Francisco Bay, California. Open-file Report. Reston (VA): US Geological Survey; p. 113.

French JR, Spencer T. 1993. Dynamics of sedimentation in a tide-dominated back-barrier salt marsh, Norfolk, UK. Mar Geol. 110:315–331.

French JR, Spencer T, Murray AL, Arnold NS. 1995. Geostatistical analysis of sediment deposition in two small tidal wetlands, Norfolk, UK. J Coastal Res. 11:308–321.

Froidefond JM, Castaing P, Jouanneau JM, Prud'Homme R, Dinet A. 1993. Method for the quantification of suspended sediments from AVHRR NOAA-11 satellite data. Int J Remote Sens. 14:885–894.

Gardner J, Dean W, Vallier T. 1980. Sedimentology and geochemistry of surface sediments, outer continental shelf, southern Bering Sea. Mar Geol. 35:299–329.

Gibbs RJ, Matthews MD, Link DA. 1971. The relationship between sphere size and settling velocity. J Sediment Petrol. 41:7–18.

Kelly M, Tuxen K. 2009. Remote sensing and geospatial technologies for costal ecosystem assessment and management. Berlin: Springer-Verlag; p. 341–363.

Krone R. 1987. A method for simulating historic marsh elevations. In: Kraus N, editor. Coastal sediments 87. New York (NY): American Society of Civil Engineers; p. 316–323.

Krumbein WC, Sloss LL. 1963. Stratigraphy and sedimentation. San Francisco (CA): W.H. Freeman; p. 660.

Li R, Kaufman Y, Gao Bo-Cai, Davis C. 2003. Remote sensing of suspended sediments and shallow coastal waters. IEEE Trans Geol Remote Sens. 41:559–566.

Looker R. 2011. Water quality control plan (basin plan) for the San Francisco Bay Region. San Francico Bay Regional Water Quality Control Board. Control Plan 2011.

Miller RL, McKee BA. 2004. Using MODIS Terra 250 m imagery to map concentrations of total suspended matter in coastal waters. Remote Sens Environ. 93:259–266.

Munday JC, Jr, Alföldi TT. 1979. LANDSAT test of diffuse reflectance models for aquatic suspended solids measurement. Remote Sens Environ. 8:169–183.

[NCDC] National Climate Data Center. 2010. National Environmental Satellite, Data, and Information Service, National Oceanic and Atmospheric Administration; [cited 2010 Jul 10]. Available from: http://www.ncdc.noaa.gov/oa/ncdc.html.

Newcomer M, Kuss A, Ketron T, Remar A, Choksi V, Grove K, Skiles JW. 2011. Modeling sediment deposition for predicting marsh habitat development. Proceedings for the American Society for Photogrammetry and Remote Sensing Conference; May 3; Milwaukee Wisconsin. Bethsesda: MD.

[NOAA] National Oceanic and Atmospheric Administration. 2011. Tides and currents. NOAA Predictions for Coyote Creek in Alviso Slough; [cited 2010 Jul 10]. http://www.tidesandcurrents.noaa.gov.

Pasternack GB, Brush GS. 1998. Sedimentation cycles in a river-mouth tidal freshwater marsh. Estuaries Coasts. 21:407–415.

Pavelsky TM, Smith LC. 2009. Remote sensing of suspended sediment concentration, flow velocity, and lake recharge in the peace-Athabasca delta, Canada. Water Resour Res. 45:1–16.

Philip Williams & Associates, Ltd. 2005. Hydrodynamics and sediment dynamics: existing conditions report. South Bay Salt Pond Restoration Project, California State Coastal Conservancy, US Fish & Wildlife Service, California Department of Fish and Game; p. 88.

Philip Williams & Associates, Ltd, Faber PM. 2004. Design guidelines for tidal wetland restoration in San Francisco Bay. The Bay Institute and California State Coastal Conservancy, Oakland, CA; p. 83.

Reed DJ. 1989. Patterns of sediment deposition in subsiding coastal salt marshes, Terrebonne Bay, Louisiana: the role of winter storms. Estuaries Coasts. 12:222–227.

Ruhl CA, Schoellhamer DH, Stumpf RP, Lindsay CL. 2001. Combined use of remote sensing and continuous monitoring to analyze the variability of suspended sediment concentrations in San Francisco Bay, California. Estuar Coast Shelf Sci. 53:801–812.

SI Metric. 2010. Mass, weight, density, or specific gravity of bulk materials. SI Metric. [online]. [cited 2010 Aug 9]. Available from: http://www.simetric.co.uk/si_materials.htm.

Siegel SW, Bachand PAM. 2002. Feasibility analysis of South Bay salt pond restoration, San Francisco Estuary, California. San Rafael (CA): Wetlands and Water Resources.

Stumpf RP, Pennock JR. 1989. Calibration of a general optical equation for remote sensing of suspended sediments on a moderately turbid estuary. J Geophys Res. 94:363–377.

Takekawa JY, Miles AK, Schoellhamer DH, Jaffe B, Athearn ND, Spring SE, Shellenbarger GG, Saiki MK, Mejia F, Lionberger MA. 2005. South Bay Salt Ponds Restoration Project. Short-term Data Needs, 2003–2005, Unpubl. Final Report, US Geological Survey, Vallejo, CA; p. 270.

Temmerman S, Govers G, Meire P, Wartel S. 2003. Modelling long-term tidal marsh growth under changing tidal conditions and suspended sediment concentrations, Scheldt estuary, Belgium. Mar Geol. 193:151–169.

Temmerman S, Govers G, Wartel S, Meire P. 2004. Modelling estuarine variations in tidal marsh sedimentation: response to changing sea level and suspended sediment concentrations. Mar Geol. 212:1–19.

Teodoro A, Veloso-Gomes F, Gonçalves H. 2008. Statistical techniques for correlating total suspended matter concentration with seawater reflectance using multispectral satellite data. J Coastal Res. 24:40–49.

Trulio L, Clarke D, Ritchie S, Hutzel A. 2007. South Bay salt pond restoration project: adaptive management plan. Final Environmental Impact Statement Report, South Bay Salt Pond Restoration Project, CA; p. 143.

USGS. 2007. Continuous monitoring in the San Francisco Bay and Delta. US Geological Survey. [online]. [cited 2010 Jun 14]. Available from: http://sfbay.wr.usgs.gov/sediment/Cont_monitoring/index.html.

USGS. 2010a. Global Visualization Viewer, Earth Resources Observation and Science Center, (Glovis); [cited 2010 Jul 10]. Available from: http://glovis.usgs.gov/.

USGS. 2010b. Water quality monitoring of San Francisco Bay. US Geological Survey. [online]. [cited 2010 Jun 14]. Available from: http://sfbay.wr.usgs.gov/access/wqdata.

Wilde IF. 2009. Neural networks, Mathematics Department, King's College London. [online]. [cited 2010 Aug 19]. Available from: http://homepage.ntlworld.com/ivan.wilde/notes/nn/nnnotespdf.pdf.

[WIST] Warehouse Inventory Search Tool. 2010. Land process distributed active archive center. National Aeronautics and Space Administration; [cited 2010 Jul 22]. https://lpdaac.usgs.gov/lpdaac/get_data/wist.

Xuejie L, Damen MCJ. 2010. Coastline change detection with satellite remote sensing for environmental management of the Pearl River estuary, China. J Mar Sys. 82:S54–S61.

Zill DG, Cullen MR, editors. 2009. Differential equations with boundary value problems, 7th ed. Belmont (CA): Brooks/Cole Cengage Learning.